

DIAGNOSIS OF INCIPIENT FAULTS IN NONLINEAR ANALOG CIRCUITS

Yong Deng, Yibing Shi, Wei Zhang

The School of Automation Engineering, University of Electronic Science and Technology of China, Chengdu, 610054, China
(✉ y_den117@126.com, +86-028-66972007, ybshi@uestc.edu.cn, weizhang@uestc.edu.cn)

Abstract

Considering the problem to diagnose incipient faults in nonlinear analog circuits, a novel approach based on fractional correlation is proposed and the application of the subband Volterra series is used in this paper. Firstly, the subband Volterra series is calculated from the input and output sequences of the circuit under test (CUT). Then the fractional correlation functions between the fault-free case and the incipient faulty cases of the CUT are derived. Using the feature vectors extracted from the fractional correlation functions, the hidden Markov model (HMM) is trained. Finally, the well-trained HMM is used to accomplish the incipient fault diagnosis. The simulations illustrate the proposed method and show its effectiveness in the incipient fault recognition capability.

Keywords: nonlinear circuits, fault diagnosis, Volterra series, fractional correlation, hidden Markov model (HMM).

© 2012 Polish Academy of Sciences. All rights reserved

1. Introduction

With the successful application of technology of testing digital parts in mixed-signal circuits, the problem how to improve the capability of diagnosing analog parts has received more attention. It is reported that 80% of the faults occur in the analog segments in mixed-signal circuits [1]. Therefore, research on the diagnosis of analog circuits has become important [2].

Fault models for analog and mixed-signal circuits can be classified into two categories: hard faults and soft faults [3]. The difference between the two kinds of faults is whether the topology of the CUT change or the nominal parameters of the analog parts vary greatly [4]. It is more difficult to diagnose soft faults than hard faults because the features of the soft fault cases of the CUT are not significant. In recent years, many methods such as the fault dictionary method [5, 6], the neural network [7-10], fuzzy analysis [11, 12], the FNLP method [13], the wavelet preprocessing [14], the test-point node selection [15], PCA method [16] and the support vector machine algorithm [17-19] have been presented for fault diagnosis of analog circuits.

However, all the aforementioned fault diagnosis methods and fault models cannot properly diagnose incipient faults. The incipient fault occurs when a parameter of the electronic component begins to change. Usually, the variation of the parameter of an incipient faulty component is small, which means that the circuit can still work and its performance begins to degrade from its normal operating state. In fact, the incipient fault is a kind of special soft fault. Comparing with the common soft fault, the variation of the parameter of the incipient faulty component is smaller, which makes it more difficult to diagnose incipient faults. For example, the incipient fault of the gain of the operational amplifier occurs when the parameter of the gain exceeds that of the parts' nominal value by [1%, 3%] while the common soft fault

of the gain of the operational amplifier can be defined within the range of [5%, 15%] exceeding the nominal values.

Based on the ideas in [20], reference [21] developed a method for diagnosing incipient faults. The reference combined HMM with LDA to obtain the incipient fault recognition capability. However, the method of [21] neglects the influence of nonlinearity in analog circuits. In practical applications, analog circuits commonly exhibit certain nonlinearities that cannot be sufficiently estimated by conventional linear models [22]. Neglecting the influence of nonlinearity will result in the failure to diagnose some incipient faults in analog circuits. Therefore, researches on nonlinearity are very important in both theory and applications.

To solve the problem of nonlinearity, this paper proposes a new technique that is suitable for incipient fault diagnosis. It is based on the fractional correlation to extract the fault features. The proposed method is made adaptive to the influence of nonlinearity. Fig. 1 shows the basic principle of the fault diagnosis method proposed in the paper. In the proposed method, the fault features of known condition of the CUT are extracted to build a fault dictionary firstly. Then, the fault features of unknown condition of the CUT are extracted and the faults are identified by HMM.

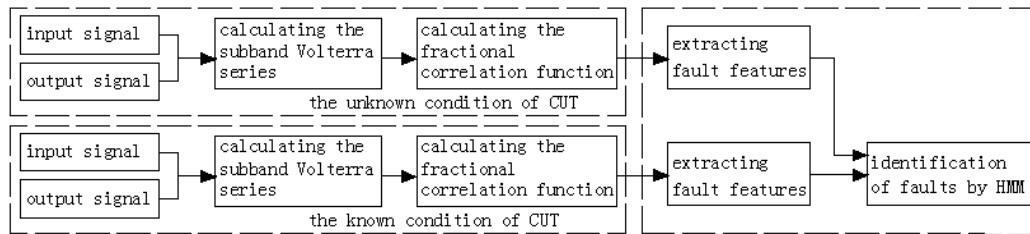


Fig.1. The block diagram of the proposed method.

The remainder of the paper is organized as follows. In section 2, the fault diagnosis method is described. The HMM is briefly reviewed and the detailed fault diagnosis steps are given in section 3. Two simulations described in section 4 test the performance of the proposed method. Finally, conclusions are drawn in section 5.

2. Fault Diagnosis Method

The Volterra kernels (called Volterra series in the discrete domain) are widely used to model nonlinear circuits as transfer functions model linear circuits [23, 24]. The Volterra kernel can characterize a class of nonlinear circuits which have the features of cause, stability and time-invariability [25]. The Volterra kernel is the fundamental feature which will not change even if input signals change. Different nonlinear circuits have different Volterra kernels. If faults occur, the Volterra kernels of the nonlinear circuit will change because the condition of the circuit has changed. In the discrete time domain, a Volterra series description of i^{th} -order nonlinearity can be defined as equation (1) [24].

$$\begin{aligned}
 y(n) &= y_1(n) + y_2(n) + \dots + y_i(n) + e(n) \\
 y_1(n) &= \sum_{m=0}^{M1-1} h_1(m)u(n-m) \\
 y_2(n) &= \sum_{m1=0}^{M1-1} \sum_{m2=0}^{M2-1} h_2(m_1, m_2)u(n-m_1)u(n-m_2) \\
 &\dots \\
 y_i(n) &= \sum_{m1=0}^{M1-1} \dots \sum_{mi=0}^{Mi-1} h_i(m_1, \dots, m_i)u(n-m_1) \dots u(n-m_i),
 \end{aligned} \tag{1}$$

where $u(n)$ and $y(n)$ are sampled versions of the continuous-time input/output signals, while $e(n)$ denotes the model error at the time instant nT (T is the sampling time interval). $h_i(m_1, \dots, m_i)$ is the i^{th} -order Volterra series where $h_1(m_1)$ and $h_2(m_1, m_2)$ represent the linear and quadratic Volterra series respectively. It should be noted that the quadratic Volterra series represents nonlinearity. $y_1(n), y_2(n), \dots, y_i(n)$ denote the output signals of the corresponding components at nT respectively. M_1, M_2, \dots, M_i are the corresponding Volterra series memorial lengths respectively.

Equation (1) is available for both fault-free and faulty cases of the CUT. The differences between fault-free and faulty cases or between faulty cases correspond to the differences between Volterra series. Owing to the dimensional disaster of Volterra models, 2nd-order Volterra-series is considered to reduce the complexity of computation [25]. If faults occur, $h_1(m_1)$ and $h_2(m_1, m_2)$ will change and different faults induce different Volterra series.

Assume $\varphi(n)$ is the discrete mother wavelet, then:

$$\varphi_{j,k}(n) = \frac{1}{2^{j/2}} \varphi\left(\frac{n}{2^j} - k\right), \quad (2)$$

where j and k are the scaling and shifting parameters respectively.

For signals $x(n) \in L^2$, the discrete wavelet representation of a signal $x(n)$ can be given as

$$x_{j,k} = \sum_{n=0}^{N-1} x(n) \varphi_{j,k}(n), \quad (3)$$

where N is the length of sequence $x(n)$ and $x_{j,k}$ is the wavelet transform of $x(n)$.

Thus $\mathbf{Y}_{1,j,k}$ can be calculated from the 1st-order output signal $y_1(n)$. ($y_1(n)$ can be calculated from $y(n)$ by the Vandermonde method).

$$\hat{\mathbf{Y}}_{1,j,k} = \mathbf{U}_{j',k'} \hat{\mathbf{H}}_{j,k,j',k'}, \quad (4)$$

where $\hat{\mathbf{Y}}_{1,j,k}$ is the estimation of $\mathbf{Y}_{1,j,k}$. $\mathbf{Y}_{1,j,k}$ and $\mathbf{U}_{j',k'}$ are the wavelet transform of $y_1(n)$ and input signal $u(n)$ respectively. $\hat{\mathbf{H}}_{j,k,j',k'}$ is the estimation of the 1st-order subband Volterra series $\mathbf{H}_{j,k,j',k'}$.

Let $y_1(n)$ and $u(n)$ are transformed with the same scaling and shifting parameters, i.e., j, j' and k, k' change in the same way. Hence, $\hat{\mathbf{H}}_{j,k,j',k'}$ can be written as $\hat{\mathbf{H}}_{j,k}$ and we can form the linear subband Volterra series sequence as equation (5).

$$\mathbf{H} = \{\hat{\mathbf{H}}_{0,0}^T, \dots, \hat{\mathbf{H}}_{0,K(0)-1}^T, \hat{\mathbf{H}}_{1,0}^T, \dots, \hat{\mathbf{H}}_{1,K(1)-1}^T, \dots, \hat{\mathbf{H}}_{j,K(j)-1}^T, \dots, \hat{\mathbf{H}}_{J-1,K(J-1)-1}^T\}, \quad (5)$$

where J is the number of the wavelet decomposition layer and $K(j-1)$ is the shifting number in the j th wavelet layer. The m th element of \mathbf{H} is written as $\mathbf{H}(m)$.

$\mathbf{Y}_{2,j,k}$ can be calculated from the 2nd-order output signal $y_2(n)$. ($y_2(n)$ can be calculated from $y(n)$ by the Vandermonde method).

$$\hat{\mathbf{Y}}_{2,j,k} = \mathbf{V}_{j',k',j'',k''} \hat{\mathbf{B}}_{j,k,j',k',j'',k''}, \quad (6)$$

where $\hat{\mathbf{Y}}_{2,j,k}$ is the estimation of $\mathbf{Y}_{2,j,k}$. $\mathbf{Y}_{2,j,k}$ is the wavelet transform of $y_2(n)$ and $\mathbf{V}_{j',k',j'',k''}$ is the 2-dimensional wavelet transform of $u(n)$. $\hat{\mathbf{B}}_{j,k,j',k',j'',k''}$ is the estimation of the 2nd-order subband Volterra series $\mathbf{B}_{j,k,j',k',j'',k''}$.

Assume that $y_2(n)$ and $u(n)$ are transformed with the same scaling and shifting parameters, i.e., j, j', j'' and k, k', k'' change in the same way. Hence, $\hat{\mathbf{B}}_{j,k,j',k',j'',k''}$ can be written as $\hat{\mathbf{B}}_{j,k}$ and we can form the quadratic subband Volterra series sequence as equation (7).

$$\mathbf{B} = \{\hat{\mathbf{B}}_{0,0}^T, \dots, \hat{\mathbf{B}}_{0,K(0)-1}^T, \hat{\mathbf{B}}_{1,0}^T, \dots, \hat{\mathbf{B}}_{1,K(1)-1}^T, \dots, \hat{\mathbf{B}}_{j,K(j)-1}^T, \dots, \hat{\mathbf{B}}_{J-1,K(J-1)-1}^T\}, \quad (7)$$

where J and $K(j-1)$ are of the same meaning as equation (5). The m th element of \mathbf{B} is $\mathbf{B}(m)$.

According to reference [26], the cross-fractional correlation function between two continuous-time functions $f_1(t)$ and $f_2(t)$ is

$$(f_1 \otimes_{\alpha} f_2)(\rho) = \int f_1^{\alpha}(\nu) [f_2^{\alpha}(\nu - \rho)]^* d\nu, \quad (8)$$

where α is the angle parameter of the Fractional Fourier Transform (FRFT) and

$$f_i^{\alpha}(\nu) = \begin{cases} \sqrt{1 - j \cot \alpha} e^{j\pi\nu^2 \cot \alpha} \int f_i(t) e^{j\pi t^2 \cot \alpha} e^{-j2\pi t \nu \csc \alpha} dt, & \alpha \neq n\pi \\ f_i(\nu), & \alpha = 2n\pi \\ f_i(-\nu), & \alpha = (2n+1)\pi \end{cases} \quad (9)$$

$i = 1, 2$

Taking into account the definition and property of FRFT [27, 28], we can derive out equation (10) from equations (8) and (9).

$$(f_1 \otimes_{\alpha} f_2)(\rho) = e^{-j2\pi\rho\rho \cos \alpha \sin \alpha/2} \int f_1(t) [f_2(t - \rho \cos \alpha)]^* e^{-j2\pi t \rho \sin \alpha} dt. \quad (10)$$

Let $\theta(\rho, \alpha) = e^{-j2\pi\rho\rho \cos \alpha \sin \alpha/2}$ and $\mathcal{G}(\rho, t, \alpha) = e^{-j2\pi t \rho \sin \alpha}$, equation (10) can be written as

$$(f_1 \otimes_{\alpha} f_2)(\rho) = \theta(\rho, \alpha) \int f_1(t) [f_2(t - \rho \cos \alpha)]^* \mathcal{G}(\rho, t, \alpha) dt. \quad (11)$$

Equation (11) is in the continuous-time domain. In the discrete domain, (11) can be written as

$$(f_1 \otimes_{\alpha} f_2)(n) = \theta(n, \alpha) \sum_m f_1(m) [f_2(m - n \cos \alpha)]^* \mathcal{G}(n, m, \alpha). \quad (12)$$

The cross-fractional correlation function can be used to describe the relation between two functions or sequences [26]. Therefore it can be used to find differences between the fault-free case and the faulty case of the CUT or between two faulty cases. Assume that \mathbf{H} and \mathbf{B} are the linear and quadratic subband Volterra series sequences of the fault-free case and \mathbf{H}_{f_i} and \mathbf{B}_{f_i} are the linear and quadratic subband Volterra series sequences of the i th faulty case. From equation (12), the fractional correlation functions of the linear and quadratic subband Volterra series sequences between the fault-free case and the faulty case of the CUT are

$$\begin{cases} FrC1(\alpha_1, n) = (\mathbf{H} \otimes_{\alpha_1} \mathbf{H}_{f_i})(n) = \theta(n, \alpha_1) \sum_m \mathbf{H}(m) [\mathbf{H}_{f_i}(m - n \cos \alpha_1)]^* \mathcal{G}(n, m, \alpha_1) \\ FrC2(\alpha_2, n) = (\mathbf{B} \otimes_{\alpha_2} \mathbf{B}_{f_i})(n) = \theta(n, \alpha_2) \sum_m \mathbf{B}(m) [\mathbf{B}_{f_i}(m - n \cos \alpha_2)]^* \mathcal{G}(n, m, \alpha_2) \end{cases} \quad (13)$$

Two fault feature variables can be constructed as

$$\begin{cases} V1(\alpha_1) = \int |FrC1(\alpha_1, n)| dn \\ V2(\alpha_2) = \int |FrC2(\alpha_2, n)| dn \end{cases} \quad (14)$$

The cross-fractional correlation function of subband Volterra series sequences represents the fundamental differences of two circuits or two conditions of the one circuit. Different faults will induce different $V1(\alpha_1)$ and $V2(\alpha_2)$. Therefore, the two variables can be used as the fault features. The formed fault features can be assessed by defining the normalized error functions as

$$\begin{cases} e(1) = \sum_{\alpha_1} (V1'(\alpha_1) - V1(\alpha_1)) / \sum_{\alpha_1} V1(\alpha_1) \\ e(2) = \sum_{\alpha_2} (V2'(\alpha_2) - V2(\alpha_2)) / \sum_{\alpha_2} V2(\alpha_2) \end{cases}, \quad (15)$$

where $e(1)$ and $e(2)$ represent the errors of the linear and quadratic fault features between two different conditions of the CUT. The values of $e(i)$ denote the degree of the difference. The bigger they are, the more significant the difference between the two different conditions of the CUT.

3. Fault Diagnosis Using HMM

A HMM is a doubly stochastic process with an underlying stochastic process that is unobservable, but can be observed through another set of stochastic processes [29]. In the fault diagnosis problem, the faulty states of the CUT are unobservable directly, i.e., they correspond to the hidden part of the HMM. The hidden states of the CUT can be observed through another set of stochastic processes that produce a sequence of uncertain test outcomes. Therefore, a HMM can provide realistic representations of the fault diagnostic process.

A HMM for the fault diagnosis can be defined by the following model notation:

(1) The state sequence $\mathbf{X} = \{\mathbf{x}_1, \dots, \mathbf{x}_t, \dots, \mathbf{x}_T\}$, where \mathbf{x}_t is the state vector at time t . $\mathbf{x}_t \in \mathbf{S} = \{\mathbf{s}_1, \dots, \mathbf{s}_i, \dots, \mathbf{s}_N\}$, $i=1,2,\dots,N$. The finite set of fault sources \mathbf{S} is associated with the faulty conditions of the CUT (including the fault-free condition) and N is the number of states of the CUT.

(2) The observation sequence $\mathbf{O} = \{\mathbf{o}_1, \dots, \mathbf{o}_t, \dots, \mathbf{o}_T\}$, where \mathbf{o}_t is the observation vector at time t . $\mathbf{o}_t \in \mathbf{\Omega} = \{\mathbf{v}_1, \dots, \mathbf{v}_k, \dots, \mathbf{v}_K\}$. The finite set of outcome $\mathbf{\Omega}$ can ascertain the integrity of faults of the CUT (including the fault-free condition) and K is the number of possible observations.

(3) The initial state distribution $\boldsymbol{\pi} = [\pi_i], \pi_i = P(\mathbf{x}_1 = \mathbf{s}_i)$.

(4) The transition probability matrix, $\mathbf{A} = [a_{ij}]$, where $a_{ij} = P\{\mathbf{x}_{t+1} = \mathbf{s}_j \mid \mathbf{x}_t = \mathbf{s}_i\}$ is the transition probability of taking the transition from state i to state j .

(5) The output probability matrix $\mathbf{B} = [b_{ik}]$ where $b_{ik} = P(\mathbf{o}_t = \mathbf{v}_k \mid \mathbf{x}_t = \mathbf{s}_i)$ is the probability of the observation, \mathbf{o}_t , at the given system state, \mathbf{x}_t .

Hence, the complete parameter set of the HMM $\boldsymbol{\Lambda} = (\mathbf{X}, \mathbf{O}, \boldsymbol{\pi}, \mathbf{A}, \mathbf{B})$ or its simplified form $\boldsymbol{\Lambda} = (\boldsymbol{\pi}, \mathbf{A}, \mathbf{B})$ can be used to express the HMM, The structure of a typical HMM is shown in Fig. 1.

The use of the HMM to solve the fault diagnosis problem requires two steps:

- 1) Training the HMM, i.e., identification of the parameters $\hat{\boldsymbol{\Lambda}} = (\hat{\boldsymbol{\pi}}, \hat{\mathbf{A}}, \hat{\mathbf{B}})$.
- 2) Testing the HMM, i.e., diagnosis of the faults using the well-trained HMM.

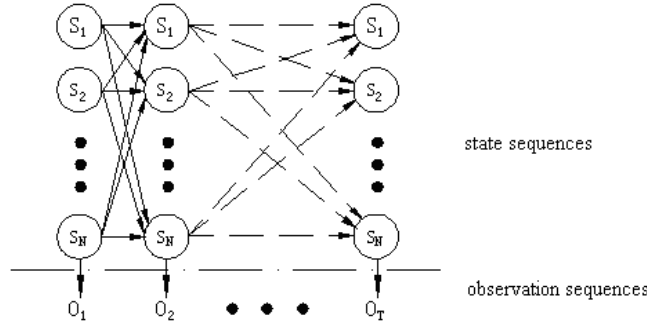


Fig. 2. The hidden Markov model (HMM).

The first step, training the HMM, can be completed by the Baum–Welch algorithm [30, 31]. This algorithm identifies the parameters $\hat{\Lambda} = (\hat{\pi}, \hat{\mathbf{A}}, \hat{\mathbf{B}})$ by maximizing the probability of the observation sequences. Assume that there are N faulty conditions and 1 fault-free condition of the CUT. There will be $N+1$ $V1(\alpha_1)$ and $V2(\alpha_2)$ which can be calculated as equation (14). In this paper, the fault features $V1(\alpha_1)$ and $V2(\alpha_2)$ are used to form the observation sequences of the HMM. Let

$$\mathbf{o}_t = \{V1(\alpha_1^1), V1(\alpha_1^2), V1(\alpha_1^3), V1(\alpha_1^4), V1(\alpha_1^5), V2(\alpha_2^1), V2(\alpha_2^2), V2(\alpha_2^3), V2(\alpha_2^4), V2(\alpha_2^5)\}, \quad (16)$$

where α_1^i and α_2^j ($i, j=1, 2, \dots, 5$) are randomly selected between the range $(0, \pi/2]$.

According to the Baum–Welch algorithm, $\hat{\Lambda} = (\hat{\pi}, \hat{\mathbf{A}}, \hat{\mathbf{B}})$ can be calculated as

$$\begin{cases} a_{ij} = \sum_{t=1}^{T-1} \gamma_t(i, j) / \sum_{t=1}^{T-1} \sum_j \gamma_t(i, j) \\ \hat{b}_{jk} = \sum_{t: \mathbf{o}_t = \mathbf{v}_k} \gamma_t(j) / \sum_{t=1}^T \gamma_t(j) & , k = 1, 2, \dots, K, j = 1, 2, \dots, N, \\ \pi_i = \gamma_1(i) \end{cases} \quad (17)$$

where

$$\gamma_t(i, j) = [\sigma_t(i) a_{ij} b_j(\mathbf{o}_{t+1}) \beta_{t+1}(j)] / \sum_{n=1}^N \sigma_t(n) \quad (18)$$

and

$$\gamma_t(i) = [\sigma_t(i) \beta_t(i)] / \sum_{i=1}^N \sigma_t(i). \quad (19)$$

The forward operator σ and the backward operator β can be modified as equations (20) ~ (23).

$$\sigma_{t+1}(j) = \left[\sum_{i=1}^N \sigma_t(i) a_{ij} \right] \prod_{k=1}^K b_j(\mathbf{o}_{t+1}(k)), t = 1, \dots, T-2, T-1, 1 \leq j \leq N, \quad (20)$$

$$\sigma_t(i) = P(\mathbf{O}_1 \mathbf{O}_2 \dots \mathbf{O}_t, \mathbf{X}_t = \mathbf{S}_i | \Lambda), \quad (21)$$

$$\beta_t(i) = \left[\sum_{j=1}^N a_{ij} \beta_{t+1}(j) \right] \prod_{k=1}^K b_j(\mathbf{o}_{t+1}(k)), t = T-1, T-2, \dots, 1, 1 \leq j \leq N, \quad (22)$$

$$\beta_{t+1}(i) = P(\mathbf{o}_{t+1} \mathbf{o}_{t+2} \cdots \mathbf{o}_T, \mathbf{X}_t = \mathbf{S}_i | \Lambda). \quad (23)$$

The recursive process does not stop until the convergence criterion is met and the parameters of the HMM $\hat{\Lambda} = (\hat{\boldsymbol{\pi}}, \hat{\mathbf{A}}, \hat{\mathbf{B}})$ are estimated.

After the $N+1$ HMMs have been trained well, the second step, testing the HMM for the fault diagnosis will be carried on. We will find the most likely state sequence \mathbf{X} that resulted in the observation sequence \mathbf{O} , which is equivalent to maximizing $P(\mathbf{O}|\mathbf{X})$. This step, training the HMM, can be completed by the Viterbi algorithm [29]. This algorithm is a recursive process as follows.

1) Initialize the well-train HMM. Let

$$\begin{cases} \delta_1(i) = \pi(i)b_i(\mathbf{o}_1) \\ \psi_1(i) = 0 \end{cases}, 1 \leq i \leq N. \quad (24)$$

2) Recursion. Let

$$\begin{cases} \delta_t(j) = \max_{1 \leq i, j \leq N} [\delta_{t-1}(j)a_{ij}]b_j(\mathbf{o}_t) \\ \psi_t(j) = \arg \max_{1 \leq i, j \leq N} [\delta_{t-1}(j)a_{ij}] \end{cases}, 2 \leq t \leq T, 1 \leq j \leq N. \quad (25)$$

The recursive process does not stop until $t=T$ and we will have $P^* = \max_{1 \leq j \leq N} [\delta_T(j)]$ and $j_T^* = \arg \max_{1 \leq j \leq N} [\delta_T(j)]$.

Therefore, $P(\mathbf{O}|\mathbf{X})$ has been maximized. By backtracking we can find the most likely state sequence \mathbf{X} associated with the observation sequence \mathbf{O} . From \mathbf{X} , we can identify the unknown condition of the CUT and diagnose the incipient faults.

4. Simulation

In this section, two simulations of nonlinear analog circuits are given to show the steps and results of fault diagnosis of the proposed method and the proposed method will be compared with other existing methods. The Daubechies 1 wavelet (DB1) is selected as the mother wavelet to calculate the subband Volterra series.

4.1. Simulation 1

In simulation 1, a band-pass filter circuit [21, 32] is analyzed. The nominal parameters for all components are labelled in Fig. 3. The tolerance of R1~R8 is 10%, that of C1~C8 is 5% and that of R9~R11 and Av1~Av5 (the gains of U1~U5) are 1% [21]. The ranges of corresponding incipient faults are listed in Fig. 3.

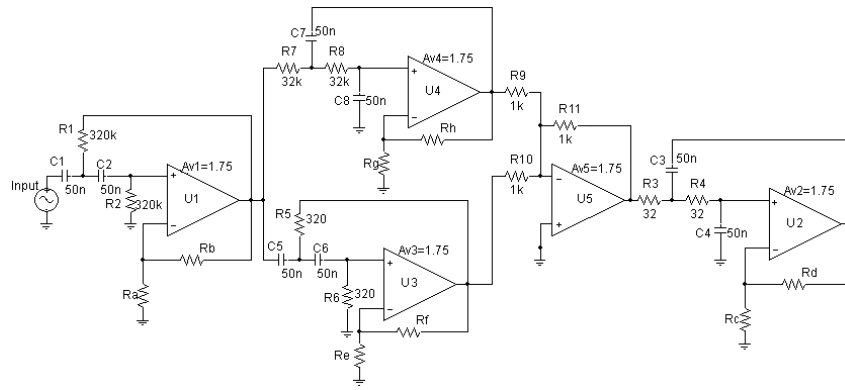


Fig. 3. Simulation 1- The band-pass filter circuit.

Table 1. Incipient faults in simulation 1.

Faulty Component	(+) Fault	(-) Fault
Fault free		
R1	[1.1Vn-1.3Vn]	[0.7Vn-0.9Vn]
R6	[1.1Vn-1.3Vn]	[0.7Vn-0.9Vn]
C2	[1.05Vn-1.15Vn]	[0.85Vn-0.95Vn]
C4	[1.05Vn-1.15Vn]	[0.85Vn-0.95Vn]
C7	[1.05Vn-1.15Vn]	[0.85Vn-0.95Vn]
R11	[1.01Vn-1.03Vn]	[0.97Vn-0.99Vn]
Av2	[1.01Vn-1.03Vn]	[0.97Vn-0.99Vn]
Av3	[1.01Vn-1.03Vn]	[0.97Vn-0.99Vn]
R9&Av1	—	R9, Av1: [0.97Vn-0.99Vn]

In Table 1, “(+) Fault” represents an increase of the component parameter and “(-) Fault” represents a decrease of the component parameter. In the following tables, the two symbols have the same meaning. Vn is the nominal parameter of the component.

Although approximating the circuit to be linear can provide good results in some cases, real circuits are not purely linear [14]. In real-world applications, theoretical linear circuits such as the band-pass filter circuit are influenced by weak nonlinearity and erroneous outputs (due to faults in the circuit) and have the possibility of being nonlinear. Therefore, the band-pass filter should be taken as a nonlinear circuit to reduce the errors of identification of the CUT.

In the simulation, the proposed method is used for the fault diagnosis of the CUT. The results of the proposed method are compared with other three methods: LDA-HMM [21], adaptive Volterra filter (AVF) [33] and the support vector machine (SVM) algorithm [19]. The stimulus is a simple 1 KHz 2Vac sinusoid voltage source for the proposed method while a complicated input stimulus is constituted by 13 test-frequency sinusoids with an amplitude of 2 for the other three methods [21]. The simple single-frequency stimulus can be used by the proposed method is that the observation vector sequences can be formed by changing the FRFT parameter α . For the other three methods, the observation vectors can only be formed by changing a different stimulus frequency.

For comparison, R1, R6, C4, C7, R11, Av3 components used in [21] will be selected as the potential faulty components in the simulation. To be more representative, other randomly selected 5 potential cases are analyzed also. They are two C2 incipient fault cases, two Av2 incipient fault cases and one R9&Av1 multiple incipient fault case. Hence, 18 cases of the CUT (17 fault cases and 1 fault-free case) are analyzed by the proposed method and compared with other methods. The cases are shown in Table 1.

Each case of the CUT is driven by the stimulus signal for $M1$ ($M1=300$ in the simulation) times respectively to implement the Monte Carlo analysis. The response voltage of each experiment is used as the output sequences, i.e., $y(n)$ in equation (1). According to the proposed method, the fault feature variables $V1$ and $V2$ can be calculated according to equation (14) and the observation vector is formed as equation (16) for each case of the CUT (altogether there are $M1$ observation vectors). In the simulation, α_1 and α_2 are set $\pi/10$, $2\pi/10$, $3\pi/10$, $4\pi/10$, $5\pi/10$ respectively. Table 2 gives the error values $e(1), e(2)$ between the fault-free case and the faulty cases. From the results in the Table, the differences between each case is clear, which is important to improve the fault diagnosis capability of the HMM used in the proposed method.

Table 2. Values (%) of $e(1)$ and $e(2)$ in simulation 1.

Fault type	$e(1)$	$e(2)$	Fault type	$e(1)$	$e(2)$
Fault-free circuit	0	0	C7(+)	153.3	652
R1(+)	44.2	84.3	C7(-)	233	367.6
R1(-)	-34.6	50.3	R11(+)	74	323.3
R6(+)	-49.8	1024	R11(-)	349.1	442.4
R6(-)	-61.9	744.2	Av2(+)	-21.3	115.8
C2 (+)	201	-68.9	Av2(-)	300.3	208.7
C2(-)	176.7	-35.5	Av3(+)	-17.2	-52
C4 (+)	103.5	253.7	Av3(-)	429.8	24.9
C4(-)	258	164.3	R9& Av1(-)	-14.6	602.7

For each circuit case, an observation sequence is formed by randomly selecting L observation vectors and $M1/L$ observation sequences are obtained to train the HMM. The detailed steps of training the HMM are according to section 4. Testing each well-trained HMM is done for $M2$ ($M2=300$ in the simulation) times by the same stimulus signal as training the HMM to complete the fault diagnosis. The results of fault diagnosis are shown in Table 3. In the same table, the results of the proposed method are compared with the results of references [21, 33, 19].

Table 3. Results of fault recognition rates (%) in simulation 1.

Fault type	The propose method	LDA-HMM[21]	AVF [33]	SVM [19]
Fault-free circuit	96.00	79.33	91.67	85.67
R1(+)	100.00	100.00	93.67	85.67
R1(-)	100.00	100.00	98.00	82.33
R6(+)	100.00	100.00	91.67	84.00
R6(-)	100.00	100.00	90.00	89.33
C2 (+)	98.33	96.00	92.33	75.33
C2(-)	97.67	97.33	90.00	71.67
C4 (+)	99.00	99.67	84.00	74.67
C4(-)	100.00	100.00	86.33	72.67
C7(+)	100.00	100.00	86.33	78.67
C7(-)	97.33	99.67	88.33	75.33
R11(+)	99.67	99.33	91.33	61.00
R11(-)	99.33	99.67	87.00	64.67
Av2(+)	94.33	51.33	51.00	56.33
Av2(-)	95.00	92.67	51.33	55.33
Av3(+)	94.33	68.33	56.00	58.33
Av3(-)	99.00	91.33	52.33	58.67
R9& Av1(-)	89.67	48.67	33.33	42.33
Mean fault recognition	97.76	90.19	78.59	70.67

From Table 3, the performance of the proposed method is superior to the other three methods with respect to fault recognition capability. The mean fault recognition rate of the proposed method is 97.76% while its worst fault recognition rate is 89.67% (in R9& Av1(-) multiple fault), which are both the best among the methods in Table 3. It shows that the proposed method can diagnose all the 18 proposed incipient faults of the CUT. The mean fault recognition rate of LDA-HMM is 91.19%, which is good enough in practical fault diagnosis. However, LDA-HMM is not good at diagnosis of the Av2(+), Av3(+) and R9& Av1(-) faults and its worst fault recognition rate is 48.67% (in R9& Av1- multiple fault), only 54% of that of the proposed method. The table also shows the performances of adaptive Volterra filter (AVF) and the support vector machine (SVM) algorithm. From the table, the incipient fault recognition capability of AVF and SVM is weaker than that of the proposed method and LDA-HMM.

The reasons that the fault diagnosis capability of the proposed method is better than the other three methods are as follows.

1) The weak nonlinearity of the CUT is considered in the proposed method while the other methods analyze the CUT as a linear circuit. When components U1~U5 are incipient faulty, the CUT is affected by the effects of the weak nonlinearity because incipient faults of U1~U5 generate a small range of parameters variation and weak nonlinearity of the CUT. However, the linear method cannot deal with the nonlinearity.

2) Due to the function of the angle parameter α , the proposed method can provide better fault feature resolution than that of the other three methods, which is helpful to improve the fault recognition capability.

3) The elements of the observation vector for the HMM in the proposed method are more independent than that of the other methods. This is because the correlation degree of different α is less than that of different frequency stimulus used by the other methods.

Let us take the instance of fault-free, Av2(+) and Av3(+) cases to give detailed and direct-viewing examples how the incipient faults are detected and isolated. Select randomly one from the *M2* test results of the three conditions of the CUT. The test results of each step are shown in Fig. 4~9. In the Figs, Av2 fault represents Av2(+) fault and Av3 fault represents Av3(+) fault.

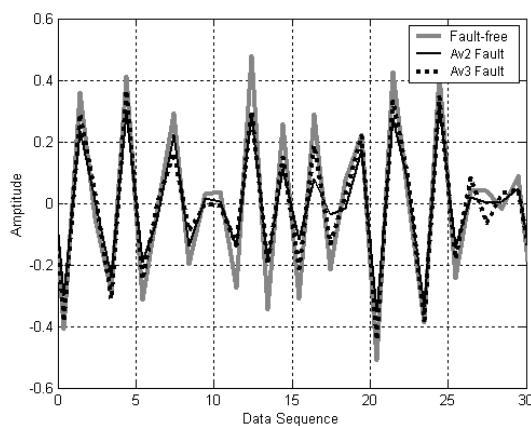


Fig. 4. Linear Volterra series in full band.

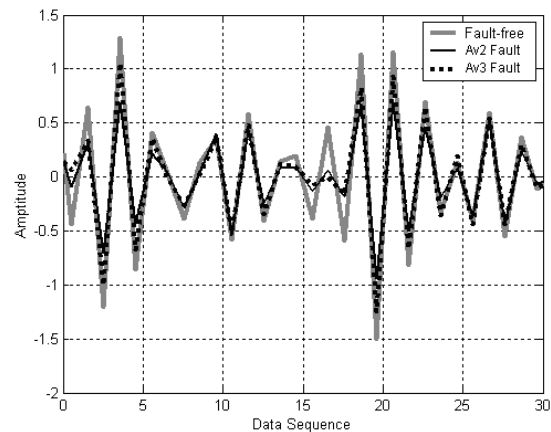


Fig. 5. Quadratic Volterra series in fullband.

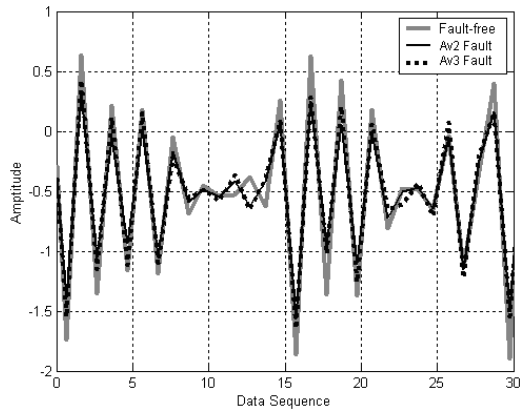


Fig. 6. Linear Volterra series in feature subband.

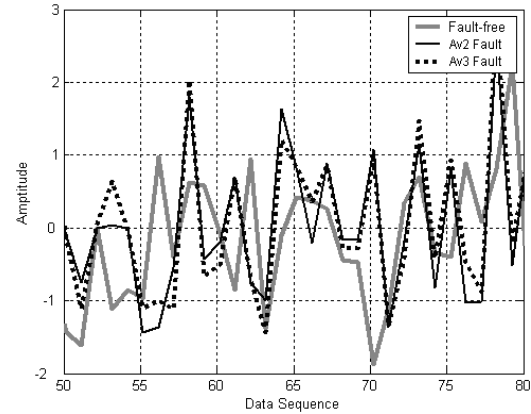


Fig. 7. Quadratic Volterra series in feature subband.

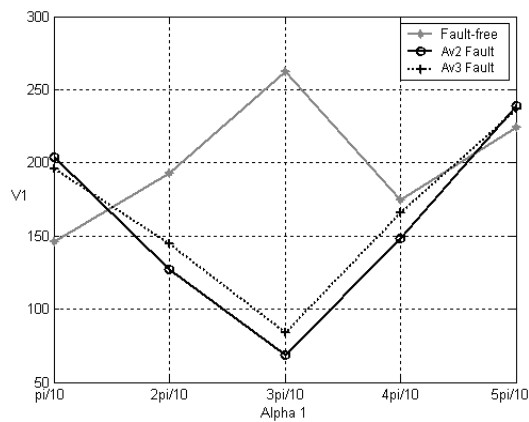


Fig. 8. The values of V1 by different α_1 .

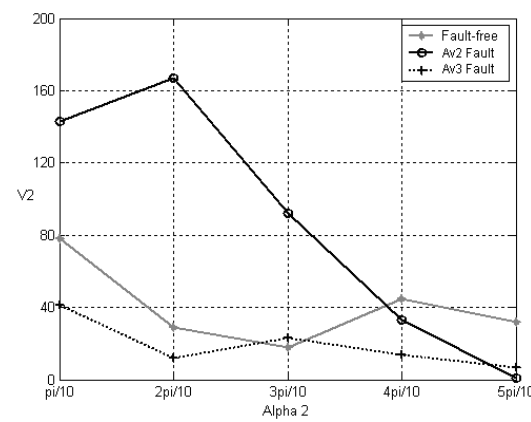


Fig. 9. The values of V2 by different α_2 .

Fig. 4~9 show the reasons why the proposed method has higher fault recognition than the other methods. Fig. 4 and 5 show the results of the linear and quadratic Volterra series in full band. The results of the three circuits are too close to make differences. Fig. 6 and 7 show the results of the linear and quadratic Volterra series in feature subband (The feature subband is the subband where the differences of the results are clearest). The differences of the results between the fault-free case and the two faulty cases of the CUT in the linear subband Volterra series are not clear while that in the quadratic Volterra series is clear. The reason is that using the linear Volterra series is the linear method as reference [21] use. As the linear method does not consider the nonlinearity, the diagnostic results of Av2(+) and Av3(+) faults are not satisfactory. Since the quadratic subband Volterra series consider the effects of the weak nonlinearity, the differences between the fault-free case and the two faulty cases of the CUT are significant. This is shown in Fig. 7.

However, the subband Volterra series cannot isolate the two faulty cases- Av2+ and Av3+ fault cases because the differences between the two subband Volterra series are not clear enough for isolation. The waveforms in Fig. 6 and 7 show the problem. In the two figures, the waveforms of the two fault cases are too close to differ from each other. Therefore, it is difficult to decide whether the fault is Av2(+) or Av3(+) even though we know that some fault has occurred.

To solve the problem, the fractional correlation function explained in section 2 in the paper is introduced. The fault features $V1(\alpha_1)$ and $V2(\alpha_2)$ are used to identify the differences between cases of the CUT. By using fractional correlation functions, the small differences between the two cases are enlarged as shown in Fig. 8 and 9. According to the two figures, we

can find that when the FRFT angle parameter $\alpha=\pi/2$, i.e. the Fourier transform is used, the difference between the two faulty cases is smallest. By changing the α value, the difference between the two faulty cases will be enlarged significantly. From the two figures, it could be noted that the values of $V1$ and $V2$ in different α_1 and α_2 are independent. Therefore, $V1$ and $V2$ can be used to form the observation vector sequence \mathbf{o}_t as equation (16) and the HMM trained by \mathbf{o}_t has higher fault recognition rates than that in [21, 33, 19]. From Fig. 8 and 9, it could also be noted that the differences between $V2$ of Av2(+) and Av3(+) cases are more significant than that between $V1$. This can be demonstrated by $e(1)$ and $e(2)$ of the two cases in Table 2.

To analyze the relation between the mean fault recognition rate and the observation vector dimension D , and the relation between the mean fault recognition rate and the testing sequence length L , some other experiments were carried out. D is set to 2, 4, 10 (D is 9 in [16]) and 20. L is set from 5 to 10. The corresponding recognition rates of the proposed method and LDA-HMM [21] is presented in Table 4 for different D and L (D and L are not used in AVF and SVM).

Table 4. Comparison of the mean fault recognition rates (%) with different D and L in simulation 1.

D	L of the proposed method						L of LDA-HMM [21]					
	5	6	7	8	9	10	5	6	7	8	9	10
2	64.3	66.9	69.1	71.4	73.2	73.8	68.7	70	71.	72.	74.	75.
								2	3	8	2	
4	74.7	77.3	78.9	81.2	83	83.2	71.2	73.	73.	74.	77.	77.
								1	9	8	3	8
10	90.3	92.3	94.8	95.2	97.4	97.7	84.6	85.	87.	87.	89.	90.
								2	1	3	7	2
20	90.8	92.7	94.5	95	97.5	97.9	85	85.	87	87.	90.	90.
								3	3	1	2	

According to Table 4, when D is small, it affects the fault recognition rate for the four methods. When D is big enough, it does not affect the fault recognition rates for the four methods. The table also shows that the mean fault recognition rate of the proposed method is better than in the other three methods when $D = 4, 10$ or 20 . This conclusion is the same as that from Table 3. Hence, D should be set ' ≥ 4 '. From the Table we can observe that the length of the testing sequence has some effect on the recognition rate, but the recognition rate of the proposed method is always higher than that of the other methods with the same length of the testing sequence when $D \geq 4$.

According to Table 3 and 4, the proposed method can diagnose the incipient faults better than the methods in [21]. The advantage of the proposed method comes mainly from considering the influence of nonlinearity and using the fractional correlation function. The detailed analysis has been given above.

4.2. Simulation 2

To show the universality of the proposed method, another nonlinear analog circuit is considered. It is a logarithm amplitude circuit as in Fig. 10. The nominal parameters for all components are labeled in the same figure. The tolerance of R1~R5 is 10%, that of C1~C2 is 5% and that of Av1~Av4 (the gains of U1, U2, T1 and T2) are 1% (The tolerance is referred as [21]). The stimulus signal is the same as in simulation 1.

15 cases are analyzed by the proposed method. The cases are shown in Table 5. The simulation conditions are the same as in simulation 1. For each circuit case, 300 observation

vectors after Monte Carlo analysis are used to form 30 training sequences and 30 testing sequences are formed in the same way for each circuit case. The diagnosis results and the comparison results of the four methods are shown in Table 5.

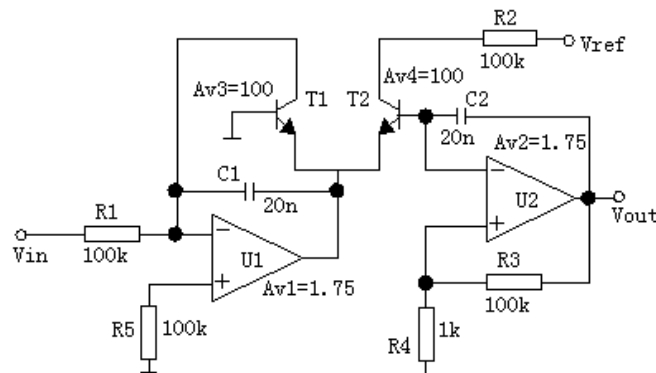


Fig. 10. Logarithm amplitude circuit in simulation 2.

From Table 5, the performance of the proposed method is higher than that of the other three methods in fault recognition capability. The mean fault recognition rate of the proposed method is 97.82% while its worst fault recognition rate is 90.33% (in Av1(+)&Av4(-) multiple fault), which are both the best among the methods in Table 5. The mean fault recognition rate of LDA-HMM is 86.31%, but it fails in the fault diagnosis of the two Av3 faults and the two multiple faults due to the low fault recognition capability in the four faults. Like simulation 1, the results of the AVF and SVM method are not satisfactory compared to the proposed method and LDA-HMM. This conclusion is the same as in simulation 1.

Table 5. Results of fault recognition rates (%) in simulation 2.

Fault type	The propose method	LDA-HMM[21]	AVF [33]	SVM [19]
Fault-free circuit	100.00	91.00	88.67	74.67
R1(+)	100.00	100.00	87.33	75.00
R1(-)	100.00	99.67	86.67	76.33
R3(+)	99.33	99.67	80.33	70.33
R3(-)	97.67	99.67	80.00	72.67
R5(+)	98.33	96.67	81.33	73.67
R5(-)	99.33	95.33	82.33	74.33
C1(+)	100	99.67	80.00	73.33
C1(-)	100	97.67	87.67	77.67
C2(+)	98.67	97.00	84.33	75.33
C2(-)	100.00	99.00	76.67	75.33
Av3(+)	95.67	67.33	62.33	61.67
Av3(-)	94.33	62.00	63.00	60.00
R2(-)&Av4(+)	93.67	48.67	38.67	45.67
Av1(+)&Av4(-)	90.33	41.33	40.67	43.33
The mean fault recognition	97.82	86.31	74.67	68.62

Table 6. Comparison of the mean fault recognition rates (%) with different D and L in simulation 2.

D	L of the proposed method						L of LDA-HMM [21]					
	5	6	7	8	9	10	5	6	7	8	9	10
2	62.2	63.9	65.9	66.7	69.1	69.4	69.7	72.2	75.7	76.5	78.1	78.9
4	75.4	77.7	80.3	80.9	83.4	83.7	71.3	73.9	75.4	76	78	80.1
10	91.8	92.6	94.9	95.3	97.6	97.8	82	82.5	85.3	84.9	85.6	86.4
20	92.	93.7	95.4	95.7	98.2	98.3	81.5	82.3	83.4	84.4	85.1	86.2

Some other experiments were carried out to analyze the relations between the mean fault recognition and the observation vector dimension D , and the relation between the mean fault recognition and the testing sequence length L . The same conditions as simulation 1 were given and the corresponding fault recognition rates of the proposed method and LDA-HMM are presented in Table 6 for different D and L (D and L are not used in AVF and SVM).

From Table 6 we can draw the conclusion that the proposed method significantly outperforms the LDA-HMM when $D \geq 4$. This is another example to show the advantages of the proposed method. To make full use of the fault recognition capability of the proposed method, D should be set to 4 or higher in practice. It could be noted that the advantages of the proposed method over LDA-HMM are more significant in simulation 2 than that in simulation 1 according to Tables 5 and 6. It is because the nonlinearity of the CUT is stronger in simulation 2 than that in simulation 1. This further proves that the methods in [21] are not fit for the diagnosis of the incipient faults in nonlinear analog circuits.

In the two experiments above, the proposed method shows good incipient fault diagnosis capability which is better than that of LDA-HMM, the neural network and the wavelet processing. It could be noted that the proposed method can diagnose both linear faulty components such as resistances, capacitors and nonlinear faulty components such as transistors. The conclusion can be drawn from the analysis of the different analog circuits above.

5. Conclusions

This paper uses a novel method to extract the incipient fault features in a nonlinear analog circuit. In the paper, we have derived an explicit subband Volterra model and constructed incipient fault features with the fractional correlation method. Using the observation sequences made up of the constructed incipient fault features, the HMM are trained and the incipient fault diagnosis in nonlinear circuits can be completed well. Simulation results show that this new scheme is more efficient than the existing methods. It is worthwhile noting that the proposed method is universal for nonlinear analog circuits.

Since calculation of the subband Volterra series and fractional correlation functions can be implemented with small hardware overhead, it is easy to use the proposed method to diagnose the incipient faulty parts in mixed-signal circuits. This provides a novel way to solve this kind of problem.

The proposed method achieves a significant improvement for the LDA-HMM [21] in analog circuits. However, considering the nonlinearity will increase the complexity of computation. Hence, it is an interesting issue to analyze the relations between improving the fault diagnosis capability and reducing the complexity of computation, which will be investigated in our future research work.

Acknowledgements

The authors would like to thank the reviewers and the editors for their constructive comments and suggestions.

This work is supported by the Program for New Century Excellent Talents in University (NCET-05-0804) and partly supported by Chinese National Programs for High Technology Research and Development.(2006AA06Z222).

References

- [1] Li, F., Woo, P.Y. (2002). Fault detection for linear analog IC—the method of short-circuits admittance parameters. *IEEE Trans. Circuits Syst.I*, 49(1), 105-108.
- [2] Huertas, I.L. (1993). Test and design for testability of analog and mixed-signal integrated circuits: theoretical basis and pragmatical approaches. *Proc. ECCTD Conf.*, 75-156.
- [3] Kondagunturi, R., Bradley, E., Maggard, K., Stroud, C. (1999). Benchmark circuits for analog and mixed-signal testing. *In: Southeastcon '99 Proc. IEEE*, 217-220.
- [4] Tadeusiewicz, M., Hałgas, S. (2011). Multiple soft fault diagnosis of nonlinear dc circuits considering component tolerances. *Metrol. Meas. Syst.*, 18(3), 349-360.
- [5] Starzyk, J.A., Liu, D., Liu, Z.H., Nelson, D.E., Rutkowski, J.O. (2004). Entropy-based optimum test nodes selection for the analog fault dictionary techniques. *IEEE Trans. Instrum.Meas.*,53(3), 754-761.
- [6] Bandler, J.W., Salama, A.E. (1985). Fault diagnosis of analog circuits. *In: Proc. IEEE*, 73(8), 1279-1325.
- [7] Grzechca, D. (2011). Soft fault clustering in analog electronic circuits with the use of self organizing neural network. *Metrol. Meas. Syst.*, 18(4), 555-568.
- [8] Mohsen, A.A.K., El-Yazeed, M.F.A. (2004). Selection of input stimulus for fault diagnosis of analog circuits using ARMA model. *Int. J. Electron. Commun.*, 58(3), 212-217.
- [9] Aminian, F., Aminian, M., Collins, H.W. (2002). Analog fault diagnosis of actual circuits using neural networks. *IEEE Trans. Instrum. Meas.*, 51(3), 544-550.
- [10] Aminian, M., Aminian, F. (2000). Neural-network based analog circuit fault diagnosis using wavelet transform as preprocessor. *IEEE Trans. Circuits Syst. II*, 47(2), 151-156.
- [11] Zhou, L.F., Shi, Y.B., Tang, J.Y., Li, Y.J. (2009). Soft fault diagnosis in analog circuit based on fuzzy and direction vector. *Metrol. Meas. Syst.*, 16(1), 61-75.
- [12] Wang, P., Yang, S.Y. (2005). A new diagnosis approach for handling tolerance in analog and mixed-signal circuits by using fuzzy math. *IEEE Trans. Circuits Syst. I*, 52(10), 2118-2127.
- [13] Zhang, W., Zhou, L., Shi, Y., et al. (2010). Soft-fault diagnosis of analog circuit with tolerance using FNLP. *Metrol. Meas. Syst.*, 17(3), 349-362.
- [14] Roh, J., Abraham, J.A. (2004). Subband filtering for time and frequency analysis of mixed-signal circuit testing. *IEEE Trans. Instrum. Meas.*, 53(2), 602-611.
- [15] Yang, C.L., Tian, S.L., Long, B., Chen, F. (2011). Methods of handling the tolerance and test-point selection problem for analog-circuit fault diagnosis. *IEEE Trans. Instrum. Meas.*, 60(1), 176-185.
- [16] Grzechca, D., Rutkowski, J., Golonek, T. (2010). PCA application to frequency reduction for fault diagnosis in analog and mixed electronic circuits. *Proc. of 2010 IEEE Int. Sym. On Circuits and Systems (ISCAS), Paris, France*, 1919-1922.
- [17] Cui, J., Wang, Y. (2011). Analog circuit fault classification using improved one-against-one support vector machines. *Metrol. Meas. Syst.*, 18(4), 569-582.
- [18] Cui, J., Wang, Y. (2010). A novel approach of analog fault classification using a support vector machines classifier. *Metrol. Meas. Syst.*, 17(4), 561-582.
- [19] Grzechca, D., Rutkowski, J. (2009). Fault diagnosis in analog electronic circuits – the SVM approach. *Metrol. Meas. Syst.*, 16(4), 583-598.

- [20] Yang, S.K. (2003). A condition-based failure-prediction and processing-scheme for preventive maintenance. *IEEE Trans. Reliab.* 52(3), 373-384.
- [21] Xu, L.J., Huang, J.G., Wang, H.J., Long, B. (2010). A novel method for the diagnosis of the incipient faults in analog circuits based on LDA and HMM. *Circuits Syst Signal Process*, 29, 577-600.
- [22] Jiang, B., Shi, P., Mao, Z.H. (2011). Sliding mode observer-based fault estimation for nonlinear networked control systems. *Circuits Syst Signal Process*, 30, 1-16.
- [23] Glentis, G.O., Koukoulas, P., Kalouptsidis, N. (1999). Efficient algorithms for Volterra system identification. *IEEE Trans. Signal Process*, 47(11), 3042-3057.
- [24] Rugh, W.J. (1981). Nonlinear system theory - the Volterra/Wiener approach. *The Johns Hopkins Univ. Press*.
- [25] Evans, C., Rees, D., Jones, L., Weiss, M. (1996). Periodic signals for measuring nonlinear Volterra kernels. *IEEE Trans. Instrum. Meas.* 45(2), 362-371.
- [26] Akay, O., Boudreaux-Bartels, G.F. (2001). Fractional convolution and correlation via operator methods and an application to detection of linear FM signals. *IEEE Trans. Signal Process.* 49(5), 979-993.
- [27] Ozaktas, H.M., Zalevsky, Z., Kutay, M.A. (2001). The fractional Fourier transform with applications in optics and signal processing. *J. Wiley*.
- [28] Almeida, L.B. (1994). The fractional Fourier transform and time-frequency representations. *IEEE Trans. signal process.*, 42(11), 3084-3091.
- [29] Rabiner, L.R., Juang, B.H. (1986). An introduction to hidden Markov models. *IEEE ASSP Mag.* 3(1), 4-15.
- [30] Yang, J., Xu, Y.S., Chen, C.S. (1997). Human action learning via hidden Markov model. *IEEE Trans. Syst. Man. Cybern. Part A, Syst. Humans*, 27(1), 34-44.
- [31] Juang, B.H., Rabiner, L.R. (1991). Hidden Markov models for speech recognition. *Technometrics*, 33(3), 251-272.
- [32] Catelani, M., Fort, A. (2002). Soft fault detection and isolation in analog circuits: Some results and a comparison between a fuzzy method and radial basis function networks. *IEEE Trans. Instrum. Meas.* 51(2), 196-202.
- [33] Trevor, G.B., Rafik, A.G., Franck, B. (2009). Nonlinear system identification using a subband adaptive Volterra filter. *IEEE Trans. Instrum. Meas.*, 58(5), 1389-1397.